Imaging thermally damaged tissue by polarization sensitive optical coherence tomography

Johannes F. de Boer, Shyam M. Srinivas, Arash Malekafzali, Zhongping Chen and J. Stuart Nelson

Beckman Laser Institute and Medical Clinic, University of California, Irvine, Irvine, California 92612

deboer@bli.uci.edu

Abstract: Polarization Sensitive Optical Coherence Tomography (PS-OCT) was used to image the reduction of birefringence in biological tissue due to thermal damage. Through simultaneous detection of the amplitude of signal fringes in orthogonal polarization states formed by interference of light backscattered from turbid media and a mirror in the reference arm of a Michelson interferometer, changes in the polarization due to the optical phase delay between light propagating along the fast and slow axes of birefringent media were measured. Inasmuch as fibrous structures in many biological tissues influence the polarization state of light backscattered, PS-OCT is a potentially useful technique to image the structural properties of turbid biological materials. Birefringence of collagen, a constituent of many biological tissues, is reduced by denaturation that takes place at a temperature between 56-65 ^{0}C, thus providing an "optical marker" for thermal damage. Images showing reduction of birefringence due to thermal damage in porcine tendon and skin are presented and demonstrate the potential of PS-OCT for burn depth assessment.

OCIS codes: (170.4500) Optical coherence tomography; (260.1440) Birefringence; (170.1870) Dermatology; (260.5430) Polarization

References and links

1. R. C. Youngquist, S. Carr, and D. E. N. Davies, "Optical coherence-domain reflectometry: a new optical evaluation technique," Opt. Lett. **12,** 158–160 (1987).
2. K. Takada, I. Yokohama, K. Chida, and J. Noda, "New measurement system for fault location in optical waveguide devices based on an interferometric technique," Appl. Opt. **26,** 1603–1606 (1987).
3. B. L. Danielson and C. D. Whittenberg, "Guided-wave reflectometry with micrometer resolution," Appl. Opt. **26,** 2836 (1987).
4. D. Huang *et al.*, "Optical Coherence Tomography," Science **254,** 1178–1181 (1991).
5. A. F. Fercher, K. Mengedoht, and W. Werner, "Eye-length measurement by interferometry with partially coherent light," Opt. Lett. **13,** 186–188 (1988).
6. J. M. Schmitt, M. Yadlowsky, and R. F. Bonner, "Subsurface imaging of living skin with optical coherence microscopy," Dermatology **191,** 93 (1995).
7. V. M. Gelikonov, G. V. Gelikonov, R. V. Kuranov, K. I. Pravdenko, A. M. Sergeev, F. I. Feldchtein, Y. I. Khanin, and D. V. Shabanov, "Coherent optical tomography of microscopic inhomogeneities in biological tissues," JETP Lett **61,** 158–162 (1995).
8. J. Welzel, E. Lankenau, R. Birngruber, and R. Engelhardt, "Optical coherence tomography of the human skin," J. Am. Acad. Dermatol. **37,** 958–963 (1997).

#5895 - $15.00 US
Received July 28, 1998; Revised September 02, 1998

9. G. J. Tearney, M. E. Brezinski, B. E. Bouma, S. A. Boppart, C. Pitris, J. F. Southern, and J. G. Fujimoto, "*In vivo* endoscopic optical biopsy with optical coherence tomography," Science **276,** 2037–2039 (1997).

10. A. M. Sergeev, V. M. Gelikonov, G. V. Gelikonov, F. I. Feldchtein, R. V. Kuranov, and N. D. Gladkova, "*In vivo* endoscopic OCT imaging of precancer and cancer states of human mucosa," Optics Express **1,** 432–440 (1997), http://epubs.osa.org/oearchive/source/2788.htm.

11. M. R. Hee, D. Huang, E. A. Swanson, and J. G. Fujimoto, "Polarization-sensitive low-coherence reflectometer for birefringence characterization and ranging," J. Opt. Soc. Am. B **9,** 903–908 (1992).

12. J. F. de Boer, T. E. Milner, M. J. C. van Gemert, and J. S. Nelson, "Two-dimensional birefringence imaging in biological tissue using polarization sensitive optical coherence tomography," Opt. Lett. **22,** 934–936 (1997).

13. M. J. Everett, K. Schoenenberger, B. W. Colston Jr., and L. B. Da Silva, "Birefringence characterization of biological tissue by use of optical coherence tomography," Opt. Lett. **23,** 228–230 (1998).

14. Z. Chen, T. E. Milner, D. Dave, and J. S. Nelson, "Optical Doppler Tomographic Imaging of Fluid Flow Velocity in Highly Scattering Media," Opt. Lett. **22,** 64–66 (1997).

15. W. V. Sorin and D. M. Baney, "A Simple Intensity Noise Reduction Technique for Optical Low-Coherence Reflectometry," IEEE Photonics Tech. Lett. **4,** 1404–1406 (1992).

16. D. J. Maitland and J. T. Walsh, "Quantitative measurements of linear birefringence during heating of native collagen," Lasers Surg. Med. **20,** 310–318 (1997).

17. J. M. Schmitt and S. H. Xiang, "Cross-polarized backscatter in optical coherence tomography of biological tissue," Opt. Lett. **23,** 1060–1062 (1998).

First reported in the field of fiber optics[1–3], optical coherence tomography (OCT) has become an important high resolution technique for biomedical imaging. OCT utilizes a Michelson interferometer with a broadband source with high spatial coherence to measure light backscattered from turbid media with high spatial resolution ($\sim 10\ \mu m$) and sensitivity (>100 dB)[4]. Although first used in ophthalmology[5] to measure intraocular distances, OCT has since been used to image, for example, skin[6–8], gastrointestinal and respiratory tracts[9], and cervical dysplasia and carcinoma *in situ*[10]. In these studies, OCT images displayed the spatially resolved magnitude of light backscattered. Except in an earlier study by Hee *et al.*[11], the polarized nature of light was not considered. Recently the first spatially resolved birefringence images of bovine tendon[12] were reported which showed that PS-OCT could determine the extent of thermal damage to collagen in response to pulsed laser exposure. Also, birefringence in myocardium was demonstrated[13]. In this paper, we illustrate the importance of polarization changes in light backscattered by demonstrating birefringence changes in slowly heated porcine tendon and thermally damaged *ex vivo* porcine skin. The reduction in birefringence is attributed to the denaturation of collagen.

Non-invasive determination of the depth of tissue injury due to thermal damage, by measuring the reduction of birefringence, could have tremendous practical value in the clinical management of burn patients. The present practice is to differentiate visually burns into first, second and third degree injuries. First degree burns, which are limited to epithelial damage (70-120 μm), heal spontaneously and do not require treatment. Third degree burns, which are complete full thickness destruction of the epidermis and dermis (>2 mm), are treated with an autologous or transplanted skin graft. A second degree burn shows destruction of the epidermis and partial destruction of the underlying dermis (0.12-2 mm). If the injury produces a superficial partial thickness burn, then it is best to allow the wound to heal spontaneously from surviving skin appendages. Conversely, if the injury produces a deep partial thickness burn, then it would be wise to skin graft the wound as soon as possible to avoid infection. The determination of burn depth by visual inspection of a superficial versus deep partial thickness injury is difficult, if

#5895 - $15.00 US Received July 28, 1998; Revised September 02, 1998

not impossible, since the distinction is on the order of several cell layers within the underlying dermis. A technique capable of distinguishing superficial versus deep partial thickness burns would be of enormous benefit to burn patients.

Figure 1 shows a schematic of the PS-OCT system used in our experiments. Light from a superluminescent diode (SLD), 0.8 mW output power, central wavelength $\lambda_0 = 856\ nm$ and spectral FWHM $\Delta\lambda = 25\ nm$, passed through a polarizer (P) to select a pure linear horizontal input state, and was split into reference and sample arms by a polarization insensitive beamsplitter (BS). Light in the reference arm passed through a zero order quarter wave plate (QWP) oriented at 22.5^0 to the incident horizontal polarization. Following reflection from a mirror attached to a piezoelectric transducer (PZT), retroreflector, and return pass through the QWP, light in the reference arm had a linear polarization at 45^0 with respect to the horizontal. The normal to the plane of the PZT driven mirror made an angle of 11^0 with respect to the incident light. The mirror on the PZT modulated the reference arm length over 20 μm to generate a carrier frequency. The PZT retroreflector assembly was mounted on a translation stage to allow for active focus tracking in the sample[14]. For improved signal to noise ratio[15], a neutral density filter (NDF) positioned in the reference arm reduced intensity noise by a factor of 50.

Light in the sample arm passed through a QWP oriented at 45^0 to the incident horizontal polarization producing circularly polarized light incident on the sample. After double passage through a lens L (f=50 mm) and the sample, and propagation through the QWP, light in the sample arm was in an arbitrary (elliptical) polarization state, determined by the sample birefringence. After recombination in the detection arm, the light was split into its horizontal and vertical components by a polarizing beamsplitter (PBS) and focused (f = 50 mm) on 25 μm pinholes placed directly in front of the detectors to detect a single polarization and spatial mode.

Two dimensional images were formed by lateral movement of the sample at constant velocity v (x-direction), repeated after each longitudinal displacement (z-direction). The carrier frequency $f \approx 6$ kHz was generated by displacing the PZT driven mirror with a 50 Hz triangular or 100 Hz sawtooth waveform. Transverse and longitudinal pixel sizes of the images were, respectively, the product of the transverse velocity v and the time duration of a single ramp of the PZT waveform (10 ms for both waveforms), and the longitudinal displacement between transverse scans. Transverse and axial image resolution were $\sim 15\mu$m and $\sim 10\mu$m, respectively, determined by the beam waist at the focal point and the coherence length of the source.

The polarization state in each arm of the interferometer was computed using the Jones matrix formalism. The horizontal A_H and vertical A_V polarized components of the interference intensity between light in the sample and reference paths were detected separately. Since light from the reference arm was split equally into the horizontal and vertical polarization states, A_H and A_V were proportional to the light amplitude fields backscattered from the sample[12],

$$A_H = \sqrt{R(z)}\cos(2k_0\Delta z + 2\alpha)\ e^{-(\Omega\Delta z/c)^2}\sin(k_0 z\delta), \tag{1}$$

$$A_V = \sqrt{R(z)}\cos(2k_0\Delta z)\ e^{-(\Omega\Delta z/c)^2}\cos(k_0 z\delta), \tag{2}$$

where Δz was the optical path length difference between the sample and reference arms of the interferometer, z the depth of light backscattered from the sample, $R(z)$ described the reflectivity at depth z_s and the attenuation of the coherent beam by scattering, $k_0 = 2\pi/\lambda_0$, $\Omega = (\Delta\lambda\pi c)/(\lambda_0^2\sqrt{\ln 2})$, c the speed of light in a vacuum, δ the birefringence given by the difference in refractive indices along the fast and slow axes of the sample ($\delta = n_s - n_f$) and α the angle of the fast optical axis measured with respect to the vertical. In addition to the carrier frequency ($\cos[2k_0\Delta z]$) within the coherence envelope ($\exp[-(\Omega\Delta z/c)^2]$), both signals oscillated with a periodicity determined by

#5895 - $15.00 US Received July 28, 1998; Revised September 02, 1998

the product of sample birefringence δ and propagation depth z that allows for PS-OCT imaging.

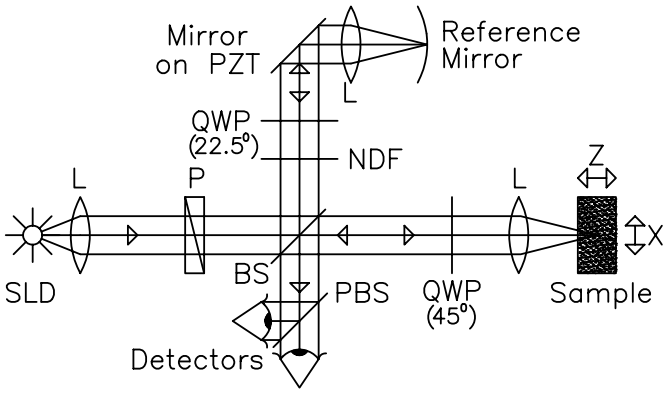

Fig. 1. Schematic of the PS-OCT system. SLD: superluminescent diode, L: lens, P: polarizer, BS: beam splitter, QWP: quarter wave plate, NDF: neutral density filter, PBS: polarizing beam splitter, PZT: Piezoelectric transducer. Two dimensional images were formed by lateral movement of the sample at constant velocity (x-direction), repeated after each longitudinal displacement (z-direction).

Signals A_H and A_V were bandpass filtered between 3-10 kHz and digitized at 5×10^4 points per second each. The central 256 points of a single ramp of the piezoelectric transducer were digitally bandpass filtered between 5-7 kHz, squared, and averaged over those 256 points (which corresponded to averaging over a 10 μm length modulation of the reference arm). The resulting signals gave the horizontal and vertical backscattered intensities as a function of depth z, modulated with their respective birefringence dependent terms, $I_H(z) = R(z)\sin^2(k_0 z\delta)$, $I_V(z) = R(z)\cos^2(k_0 z\delta)$. OCT images were formed by grayscale coding the common log of the sum of both polarization channels, $I_S(z) = I_H(z) + I_V(z)$, from 0 dB to just above the noise level, where the 0 dB level corresponded to the maximum signal in an image and the noise level was determined by the signal above the sample surface. The PS-OCT images were formed by grayscale coding the birefringence induced phase retardation,

$$\phi = \arctan\sqrt{I_H(z)/I_V(z)} = k_0 z\delta \tag{3}$$

from 0^0 to 90^0. Contour lines indicating 30^0 and 60^0 phase retardation levels in the PS-OCT images were calculated after low pass filtering by convolving the images with a Gaussian filter of 4×4 pixels and overlayed with the original image.

To investigate the effect of temperature on collagen birefringence, porcine tendon (predominantly type I collagen) was mounted in a rose chamber, filled with 5% saline solution. A thermocouple monitored the temperature inside the chamber. A heating device was mounted outside the chamber that could increase the temperature inside to 77 ^{0}C. Lateral scan velocity v (x-direction) was 100 $\mu m/s$, axial number of scans was 200, at 2 μm increments, giving an image size of 200 $\times$ 400 μm and a pixel size of 1 $\times$ 2 μm. Figure 2 shows the OCT and PS-OCT images of slowly heated tendon at 25, 45, 55, 60, 70 and 77 ^{0}C, respectively. Image acquisition was started after the rose chamber had reached the target temperature (15 to 30 minutes between consecutive scans). The last scan was taken after the sample was heated for 5 hours at 77 ^{0}C.

The images at 25, 45 and 55 ^{0}C (Figs. 2 a, b and c, respectively) showed no changes in the birefringence. The more closely spaced the banded structure, the larger the birefringence, since the accumulated phase retardation is the product of depth z and birefringence δ. At 60 ^{0}C (Fig. 2d) a reduction in the birefringence can be observed.

#5895 - $15.00 US
Received July 28, 1998; Revised September 02, 1998

The tendon shrunk considerably along the axis of the fibers during the scan, which contributed to motion artifacts in the image. At 70 ^{0}C (Fig. 2e) the birefringence is reduced further, and after 5 hours at 77 ^{0}C (Fig. 2f) the birefringence is completely gone, due to excessive thermal damage. Since Maitland *et al.*[16] have shown that the reduction of birefringence in rat tail tendon is a function of both temperature and time, no quantitative conclusions on the reduction of birefringence as a function of temperature alone can be drawn. However, the presented images demonstrate the capability of PS-OCT to measure the birefringence reduction in collagen due to thermal damage.

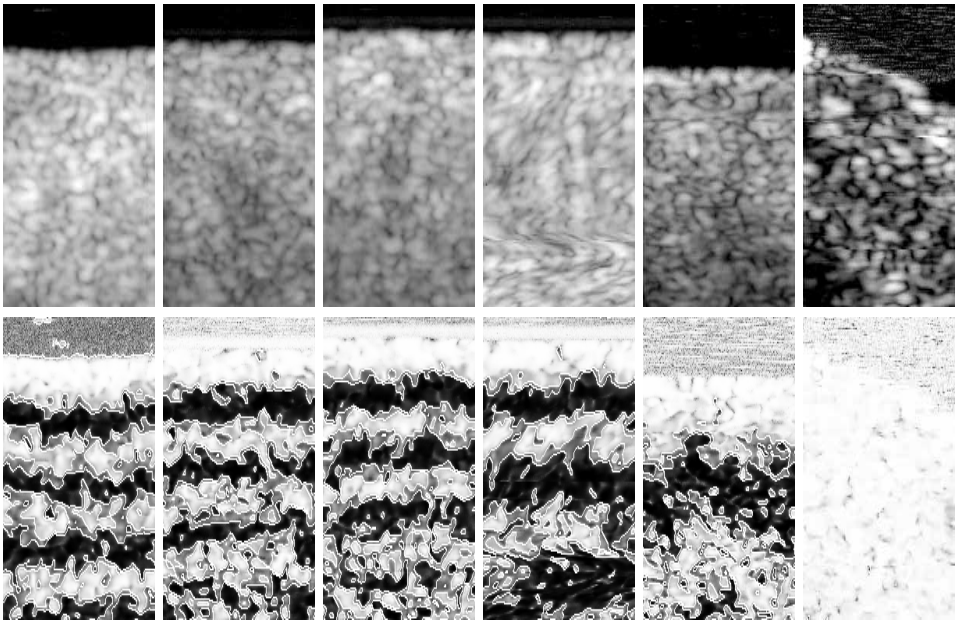

Fig. 2. OCT and PS-OCT images of porcine tendon, slowly heated in a rose chamber. Image size: 200 × 400 μm, pixel size 1 × 2 μm. Upper panel: OCT images, Lower panel: PS-OCT images. Temperature and dynamic range: a) 25 ^{0}C, 47 dB, b) 45 ^{0}C, 46 dB, c) 55 ^{0}C, 46 dB, d) 60 ^{0}C, 43 dB, e) 70 ^{0}C, 36 dB, and f) 77 ^{0}C, 25 dB. White lines in PS-OCT images are contours at 30^0 (white to gray transition) and 60^0 (gray to black transition) phase retardation levels, respectively.

Figure 3 shows OCT and PS-OCT images of normal and thermally damaged *ex vivo* porcine skin (created by applying for 10 sec. a brass rod preheated to 90^0 C). Lateral scan velocity v (x-direction) was 200 $\mu m/s$, axial number of scans was 200, at 4 μm increments, giving an image size of 400 × 800 μm and a pixel size of 2 × 4 μm. In the PS-OCT image of normal skin dark areas are visible indicating a change in the polarization state of light backscattered from the tissue. We attribute the changes to the birefringence of collagen in the skin. Since collagen is not as ordered in skin as the tendon, but randomly oriented in the dermis, the banded structure in Figs. 2 typical for the PS-OCT images is not observed. In thermally injured skin the changes in the polarization are reduced when compared to normal skin. We attribute this to the reduced birefringence of the thermally damaged collagen.

Figure 4 shows OCT and PS-OCT images of normal and thermally damaged *ex vivo* porcine skin. Lateral scan velocity v (x-direction) was 1000 $\mu m/s$, axial number of scans was 100, at 10 μm increments, giving a pixel size of 10 × 10 μm and an image size of 5 × 1 mm. The images depict, from left to right, a burned region (created by applying for 10 sec. a brass rod preheated to 300^0 C), a region corresponding to radial

#5895 - $15.00 US
Received July 28, 1998; Revised September 02, 1998

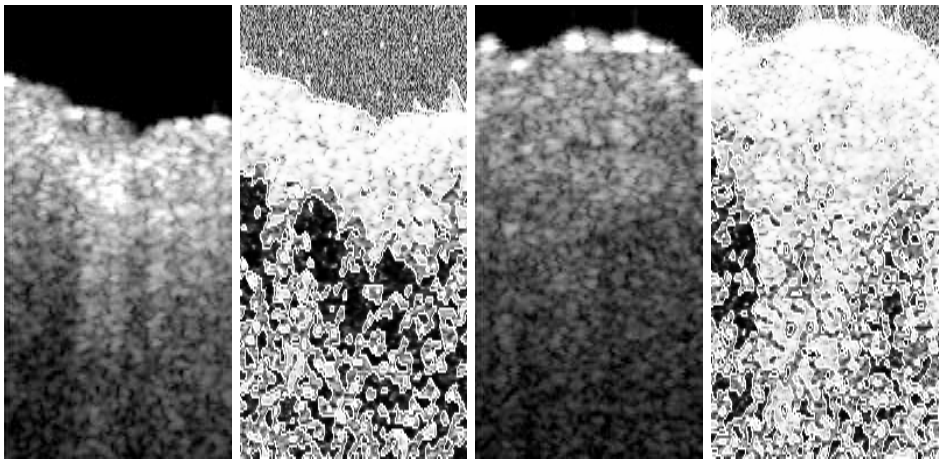

a b c d

Fig. 3. OCT and PS-OCT images of *ex vivo* porcine skin. Image size: 400 × 800 μm, pixel size 2 × 4 μm. a) OCT image of normal skin, dynamic range 40 dB, b) PS-OCT image of normal skin, c) OCT image of thermally damaged skin, dynamic range 40 dB, d) PS-OCT image of thermally damaged skin. White lines in the PS-OCT images are contours at 30^0 (white to gray transition) and 60^0 (gray to black transition) phase retardation levels, respectively.

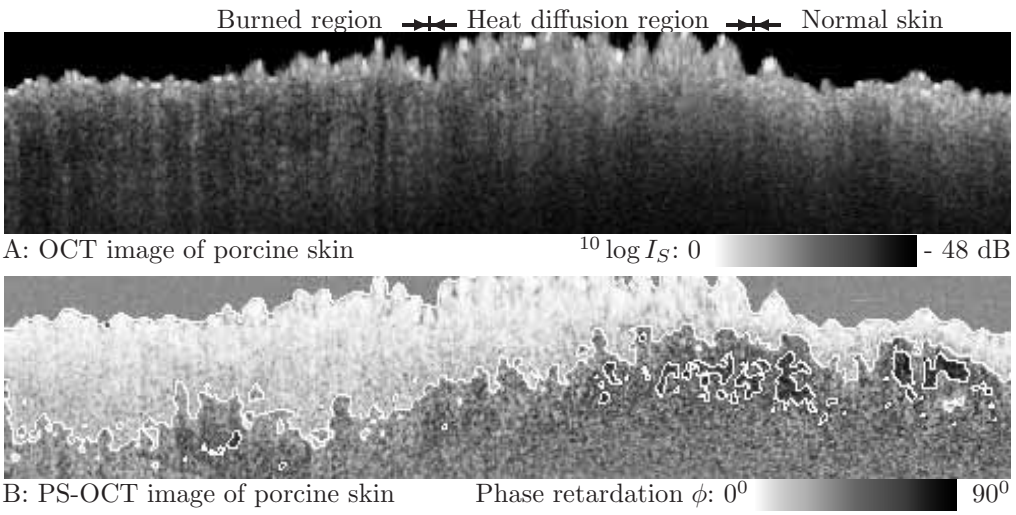

Fig. 4. OCT and PS-OCT images of *ex vivo* porcine skin. Image size: 5 × 1 mm, pixel size 10 × 10 μm. From left to right, a burned region, a region of radial heat diffusion, and normal skin. Upper panel shows OCT image, dynamic range was 48 dB. Lower panel shows PS-OCT image. White lines are contours at 30^0 (white to gray transition) and 60^0 (gray to black transition) phase retardation levels, respectively.

heat diffusion, and normal skin. Evidence of thermal injury is observed in the PS-OCT image, which shows a reduced change of the polarization in the dermis, and is clearly highlighted by the 30^0 phase retardation contour line. The differences between burned and normal skin are obvious in the PS-OCT image.

Alternatively, as was recently proposed by Schmitt and Xiang[17], the changes in the polarization could be attributed to single scattering from nonspherical particles

#5895 - $15.00 US
Received July 28, 1998; Revised September 02, 1998

and multiple scattering by particles with sizes much larger than the wavelength. Consequently, the reduced changes in the polarization in thermally injured porcine skin (Figures 3d and 4b) must be due to a change in the scattering properties of the thermally injured tissues. Figure 5 shows the averages over 100 depth profiles recorded in the normal skin (extreme right one millimeter) and the burned region (extreme left one millimeter) of Figure 4a. The depth profile recorded in the burned region shows an exponential decay in the first 200 μm that is larger than in the normal skin, followed by a weaker decay in the last 600 μm, which suggests that scattering or absorption is higher in the first 200 μm of burned skin, followed by less scattering or absorption. In both normal and burned skin at larger depths the polarization will randomize due to multiple scattering. The higher scattering observed at shallow depth in the burned skin could explain the reduced polarization changes if it is due to increased scattering by particles with sizes on the order of the wavelength or smaller. Also increased absorption could explain the reduced polarization changes by reducing the contribution of multiple scattered light to the OCT signal. The data presented in Figure 5 is not conclusive with respect to the origin of the polarization changes observed and further study is necessary.

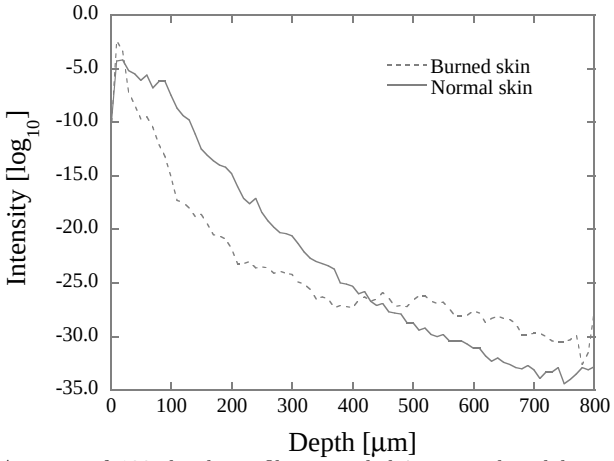

Fig. 5. Average of 100 depth profiles recorded in normal and burned porcine skin. Solid line: Normal skin, averages were calculated from the extreme right one millimeter in Figure 4a. Dashed line: Burned skin, averages were calculated from the extreme left one millimeter in Figure 4a. Averages were calculated from depth profiles starting at the tissue surface.

In summary, PS-OCT offers a non-contact technique for spatially resolved birefringence imaging that reveals thermal damage due to denaturation of collagen in porcine tendon. Similar changes in the polarization were observed in thermally injured porcine skin, which could be attributed to a reduction of birefringence, or a change in the scattering properties. Irrespective of the mechanism, the changes in the polarization between the normal and the thermally injured skin are evident in the PS-OCT images. OCT images (that map tissue reflectivity) do not show as clear a difference between normal and thermally injured skin. Clinically, PS-OCT has the potential to image rapidly the structure of burned human skin over large areas which would be of enormous benefit to burn patients.

Research grants from the Institute of Arthritis, Musculoskeletal and Skin Diseases (1R29-AR41638-01A1 and 1R01-AR42437-01A1), Whitaker Foundation (23281) and the National Center for Research Resources at the National Institutes of Health (Laser Microbeam and Medical Program, RR-01192), U.S. Department of Energy (DE-FG03-91ER61227), Office of Naval Research (N00014-94-1-0874) and the Beckman Laser Institute Endowment are gratefully acknowledged.

#5895 - $15.00 US Received July 28, 1998; Revised September 02, 1998